2022 IEEE Texas Symposium on Wireless and Microwave Circuits and Systems (WMCS) | 978-1-6654-8609-5/22/$31.00 ©2022 IEEE | DOI: 10.1109/WMCS55582.2022.9866229

Achieving Near-Constant Beamwidth and Symmetry in Patterns of the Pyramidal Ridged Horn Antenna for UAV-Based In-situ Characterization and Measurement of Phased Array Radars

Syed S. Jehangir and Jorge L. Salazar-Cerreno
Advanced Radar Research Center (ARRC)
School of Electrical and Computer Engineering (ECE)
The University *of* Oklahoma, Norman, OK, 73019 USA
{syed.s.jehangir-1, salazar}@ou.edu

***Abstract*— To take benefit from the wide bandwidth operation of the ridged horn antennas and to overcome its limitation of wider beamwidth performance at low frequencies, we propose two techniques that are used to reduce the H-plane beamwidth of the ridged horn antenna from 2 GHz to 12 GHz. For Unmanned Aerial Vehicles (UAVs) based in-situ characterization and measurement of radars, it is usually desired that the probe has narrow beamwidth as well as overall symmetric radiation patterns so that the antenna performance is not degraded due to the back-scattering from the drone structure. This is verified from the measured results that at low frequencies, when the beamwidth is wider, the fields strongly interact with the drone platform thus induces ripples in the co-polar patterns and also increases the cross-polarization levels, especially in the H-plane. To overcome this limitation, two techniques are discussed in this work. The first technique involves the integration of a wideband multi-layer dielectric lens structure with a ridged horn antenna. In the second technique, corrugations are introduced to reduce the H-plane beamwidth for the entire band of operation. Both lens and corrugations reduce the H-plane half-power beamwidth (HPBW) by around 70% (for instance at 3 GHz) and show almost similar performance within the entire frequency band. However, compared to the corrugation technique, integrating a the dielectric lens will further increase the weight of the probe and would thus degrade the flight performance of the drone due to its payload limitations. Moreover, dielectric materials are lossy and fabrication and integration of the multi-layer lens can be challenging. In such a case, using corrugations to reduce the beamwidth can be a useful technique.**

***Keywords*—wideband antenna, beamwidth, symmetric patterns, UAV, meteorology, phased array radars, outdoor measurements,**

I. Introduction

To test and characterize antenna arrays inside the anechoic chamber has been a standard for a couple of decades. There are also outdoor test ranges for testing antenna arrays, but they are costly and have some limitations. Both of these indoor and outdoor measuring platforms usually do not include the effects of the system on which the array is mounted/integrated, radome, and environmental factors such as rain, snow, ice, and pollution, etc. With the advent of Unmanned Aerial Vehicles (UAVs), in-situ characterization and measurement of radars can provide very precise data that can be crucial for weather scientists [1], [2]. Moreover, using UAV's, characterization of the radars can be done in various modes such as cylindrical or even spherical, that can provide extra freedom and useful information which is not usually possible in case of the stationary measurement platforms.

Several works can be found in literature using UAVs for antenna characterization [3]–[16]. Choosing a suitable probe[1] for UAV-based characterization requires the evaluation of the RF as well as the flight performance. For instance a bulky horn is not suitable to be mounted on UAV's due to its size and weight constraints. The authors of [10] and [11] have done a detailed study on choosing a right probe for UAVs. It is concluded that dipole and patch antennas showed worst case RF performance due to their non-directional radiation patterns which strongly interfere with the drone structure. However, as these antennas are light weight, they showed good flight performance. On the other hand, horn antenna exhibited very good radiation performance due to its comparatively narrow beamwidth and the flaring structure. However, due to the weight constraints, it showed poor flight performance. [1]

Based on this study of [10] and [11], we propose a ridged horn antenna for UAV applications. Ridged horn antennas are famous for their reduced size, low weight, and wideband operation and can be found suitable for UAV-based in-situ measurements. The wideband performance of the ridged horn antenna can also replace the need for using several probes for characterization of the radars in multiple bands. However, ridged horn antennas or in general horn antennas suffer from the wider beamwidth performance especially at low frequencies. As the beamwidth of the antenna is related to its aperture, achieving narrow beamwidth at low frequencies is challenging as it would require large aperture size. However, for UAV-based applications, increasing the aperture size would increase the weight and thus degrade the flight performance.Therefore, in this work, the authors propose two simple techniques that can be used to reduce the half-power beamwidth and to achieve near-symmetric patterns within the band of operation. The

[1]probe here refers to the ridged horn antenna.

978-1-6654-8609-5/22/$31.00 ©2022 IEEE

TABLE I: System specifications.

Category	Specifications	Value
UAV	Model/Maker	Matrice 600P/DJI
Platform	Dimensions	1.66 m x 1.52 m x 0.727 m
	Weight (no payload)	10 kg
	Max. takeoff weight	15.5 kg
	Position accuracy	GPS: $\pm$5.5 m to $\pm$0.5 m
	Position accuracy	RTK: $\pm$1 cm to $\pm$2.0 cm
	Max. angular velocity	Pitch: 300°/s, Yaw: 100°/s
	Max. pitch angle	25°/s
	Max. ascent speed	5 m/s
	Max. descent speed	3 m/s
	Max. serv. ceiling	2500 m
	Hovering time	20 min
	Operating temp.	-10°C to 40°C
Gimbal	Model/Maker	Ronin-MX/DJI
	Operation modes	Free, Follow, FPV
	Dimensions	28 cm x 34 cm
	MIU	Independent
	Connectivity	Bluetooth/USB
	Operation. Freq.	2.4 GHz
	Running time	3 hrs
	DC voltage	12 VDC
	Operating temp.	-15°C to 50°C
Antenna	Model/Maker	Dual-ridged (SH2000)/SATIMO
Probe	Frequency	2 GHz-32 GHz
	Beamwidth	160° -25° (H-planes)
	Beamwidth	110°-25° (E-planes)
	Gain	2.2 dB-16 dB
	Return loss	7 dB - 10 dB @ (2 GHz-32 GHz)
	Dimensions	4.13 in x 2.4 in x 4.1 in
	Weight	$\approx$ 1.1 lbs
Transmitter	Model/Maker	Windfreak technologies
	Freq. operation	10 MHz to 32 GHz
	Tx. power	20 dBm (CW)
	Dynamic range	50 dB
	Amplitude resol.	0.01 dB
	Phase resol.	0.01°
	Dimensions	4 cm x 4 cm x 2 cm
	DC voltage	12 VDC
	Weight	< 0.1 lb

proposed lens or corrugations reduces the H-plane beamwidth by around 70% in the low frequency band from 2-6 GHz. Since the pattern in the E-plane is not significantly affected, reducing only the H-plane beamwidth, helps in achieving overall symmetry in the patterns.

II. Antenna and System Description

The proposed measurement setup that includes the DJI Matrice 600 drone, Gimbal, CW transmitter and a SH2000 (SATIMO) dual ridged probe, was used inside the Advanced Radar Research Center's (ARRC) far-field anechoic chamber, from 2-12 GHz. On the receiver side, a similar SH2000 dual ridged probe was used as an AUT. The details of the proposed meteorology platform are summarized in Table. I.

For the purpose of analysis on the beamwidth reduction and achieving symmetry in the radiation patterns, a similar probe was modeled in HFSS^{TM}. The antenna was tuned to operate between 2 GHz and 12 GHz in order to cover our interested S, C, and X radar bands. However, to get even more wider operational bandwidth, the ridges, feed, and the back-cavity can be further optimized to get a bandwidth from 2-32 GHz, similar to the SATIMO SH2000. However, the goal of the study was to analyse and then reduce the half-power beamwidth in the lower frequency band from 2-10 GHz, where, originally the beamwidth is wider and not suitable for UAV-based in-situ characterization and measurements.

Fig. 1 shows the geometry models of the standard, lens integrated, and corrugated dual ridged horn antennas, used in this study. For the purpose of illustration, this figure also shows the E-field (V/m) distribution on the aperture of the antenna for each case, at 6 GHz. From the aperture field distributions, it can be observed that in case of the standard dual ridged horn antenna, the fields are not symmetric in the E and H-planes. If these fields are projected to a radiation pattern, it can be seen that the beamwidth is wider in the H-plane compared to the E-plane for a standard dual ridged horn antenna, as can be noticed in Table. I, where at low frequency of 2 GHz, the beamwidth in the H-plane is around 160°, while it is around 110° in the E-plane. Fig. 1 (b) shows the case when the proposed multi-layer dielectric lens is integrated with a dual-ridged horn antenna. The fields distribution shows a nearly symmetric behavior in both E and H-planes. There is however some spillover radiation from the edges of the lens, which can be corrected by either slightly increasing the size of the lens or by slightly adjusting the focal point of lens. For the third case, in which plates of the standard dual ridged horn antenna were corrugated as shown in Fig. 1 (c), near-symmetric behavior is also observed compared to the standard horn case.

From comparison of the lens and the corrugated cases, lens integrated horn exhibits more symmetric fields distribution compared to the corrugated case. However, fabrication of the multi-layer stack up of the lens will be a challenging and comparatively less accurate choice . Moreover, the dielectric based lens will have some material losses and will also increase the overall weight of the probe and thus can affect the flight performance of the drone. Thus, from this analysis, a corrugated ridged horn seems to be a good choice. In future, both lens and corrugated horns are planned to be fabricated and rigorously tested for radiation as well as flight performance, which can further justify the selection of the suitable technique for UAV-based in-situ characterization of radars.

Fig. 2 shows the lens integrated ridged horn antenna prototype mounted on a DJI Matrice 600 drone. The profile of the multi-layer lens structure is also shown. The lens dielectric profile is symmetric where the central layer has the highest permittivity. This is inspired from a Luneburg type lens configuration. The outer layers have permittivity values of close to the air so that the reflections between the air-dielectric layer are minimized. One important observation was made related to the dielectric profile of the lens. The smaller the dielectric gradient profile, the smaller are reflections between each layers and thus high gain and low sidelobe levels can be achieved. However, this also depends on the availability of the material with the required values of the dielectric constant. To design such a material, an artificial technique can be used to achieve the desired values of the dielectric constant for each layer of the lens structure according to [17]. Fig. 2 also shows the detailed description of the ridged horn antenna and the corrugation along with some of their dimensions. The antenna is fed using 50 Ω coaxial feeding backed by the metallic

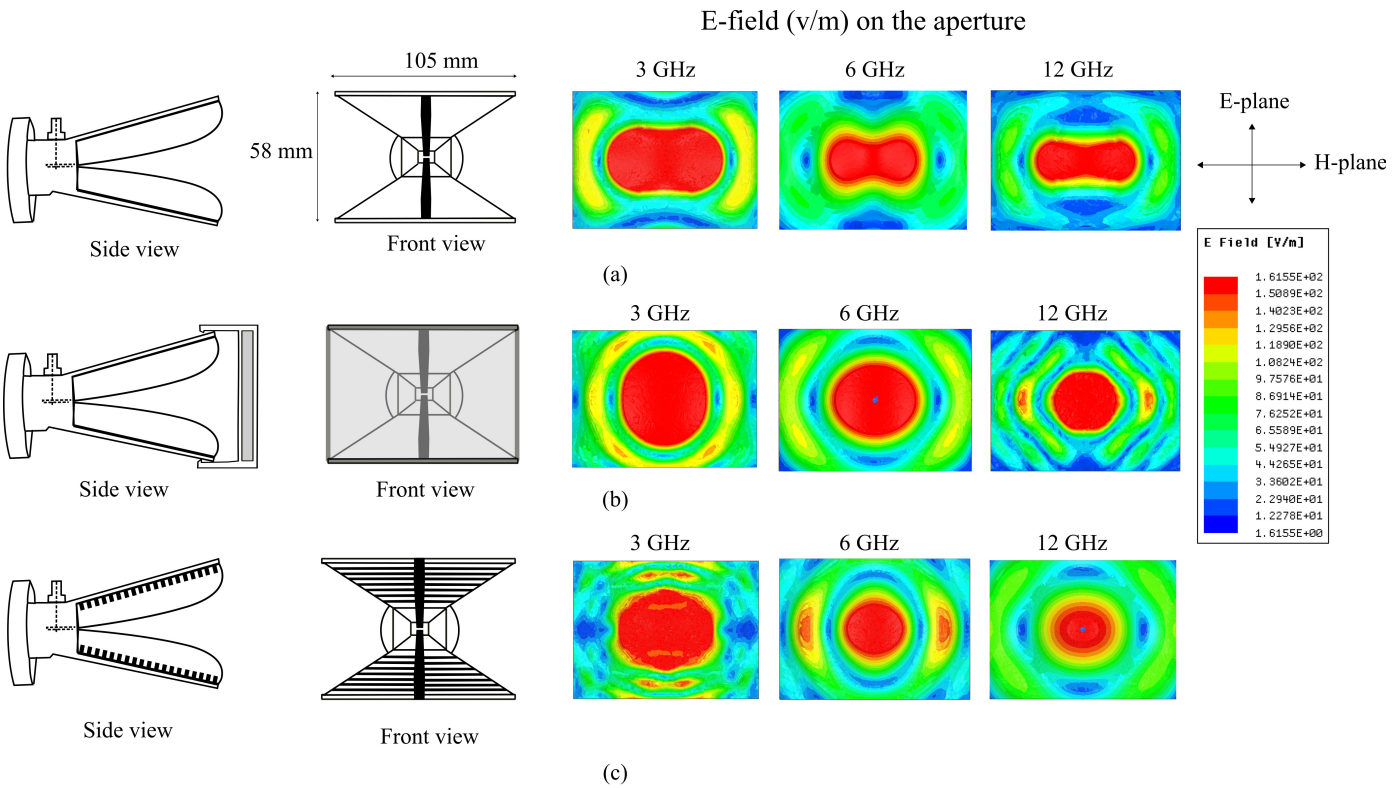

Fig. 1: Antenna geometry models and E-field distribution on the antenna aperture at different frequencies (a) standard dual-ridged horn antenna without lens or corrugations (b) lens integrated dual-ridged horn antenna (c) corrugated dual-ridged horn antenna.

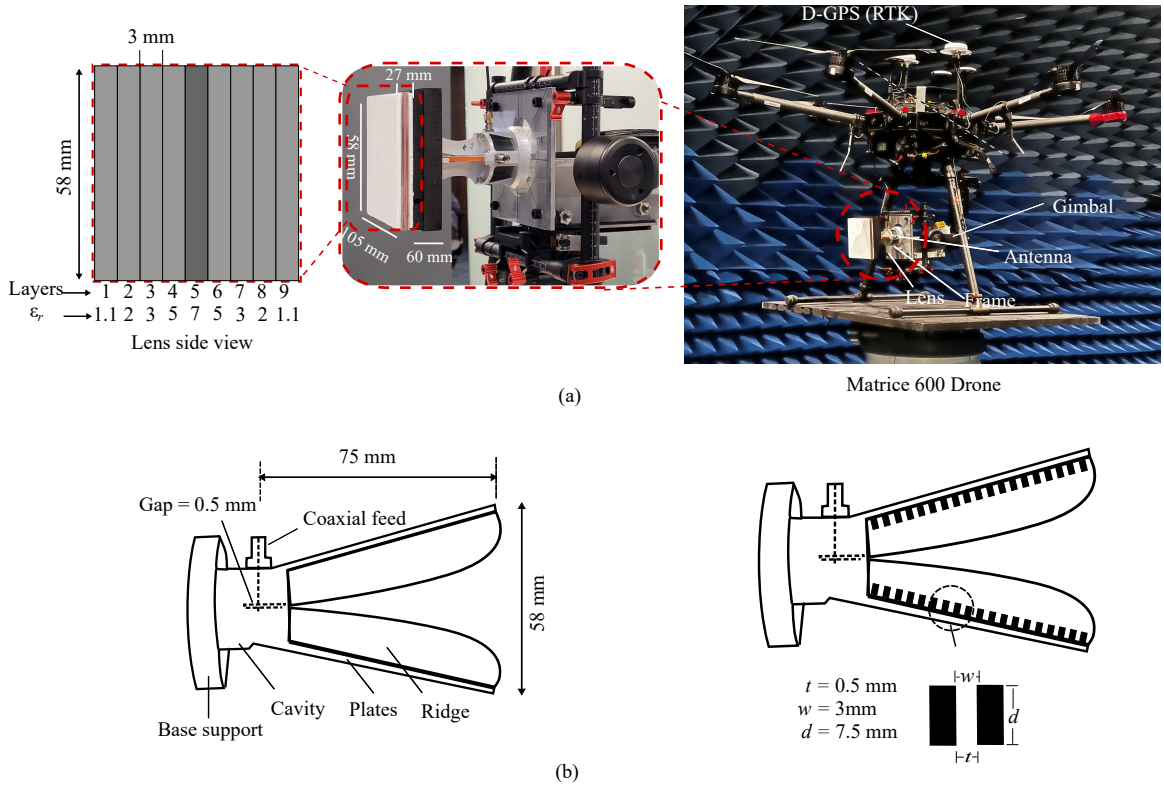

Fig. 2: Description of the DJI Matrice 600 drone carrying the ridged horn antenna (a) prototype of the lens integrated ridged horn antenna mounted on the drone (b) description and dimensions of the standard and corrugated horn antennas.

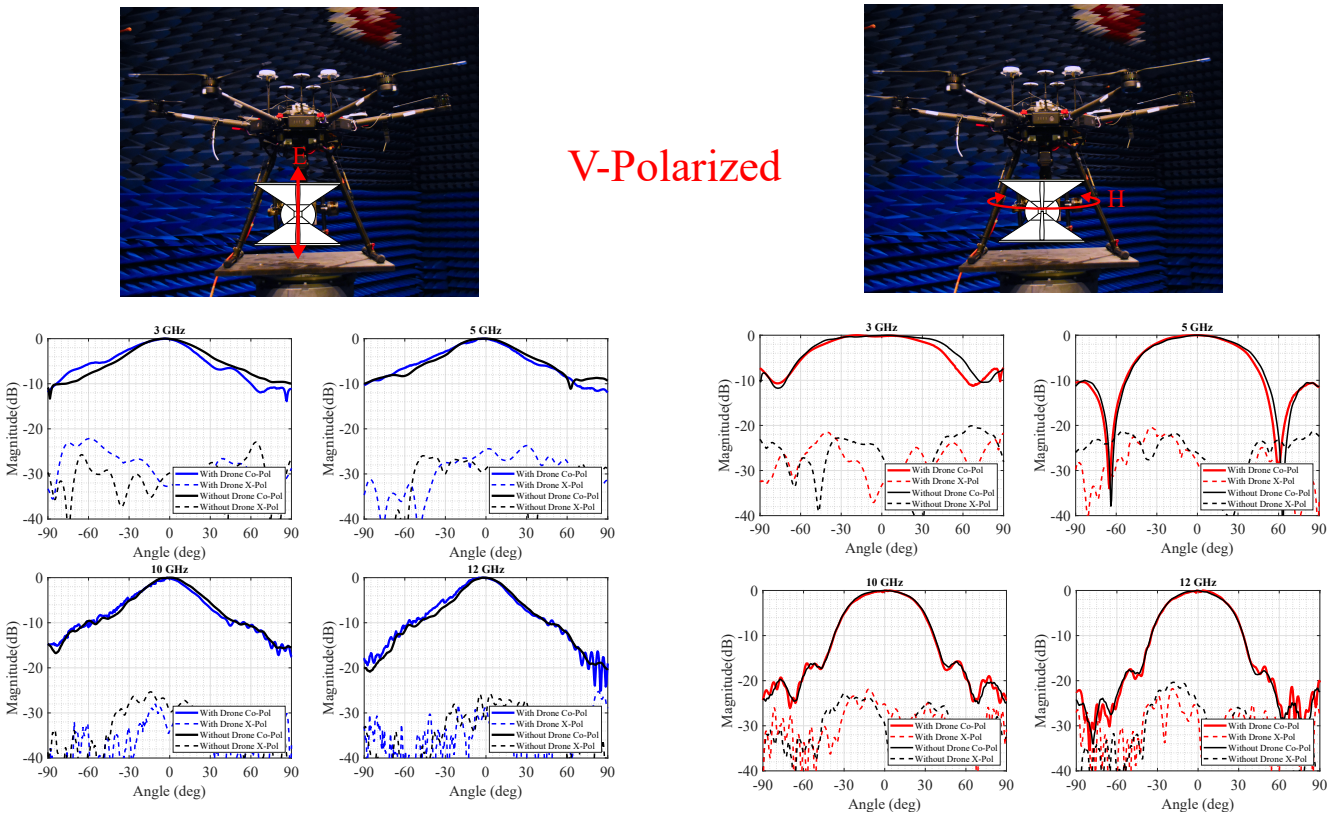

Fig. 3: Comparison of the measured radiation patterns in E and H planes at different frequencies, when the antenna is vertically polarized (V-Polarized) .

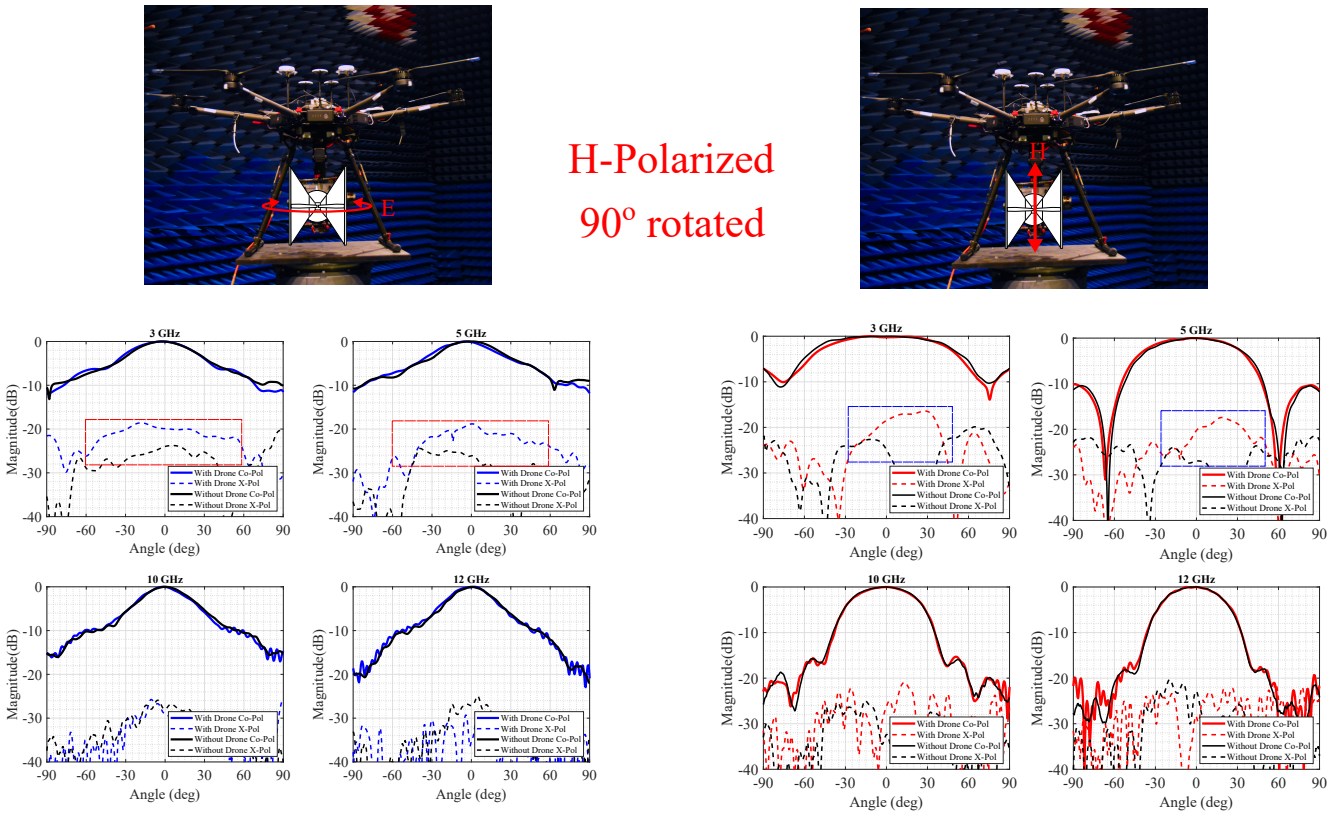

Fig. 4: Comparison of the measured radiation patterns in E and H planes at different frequencies, when the antenna is horizontally polarized (H-Polarized).

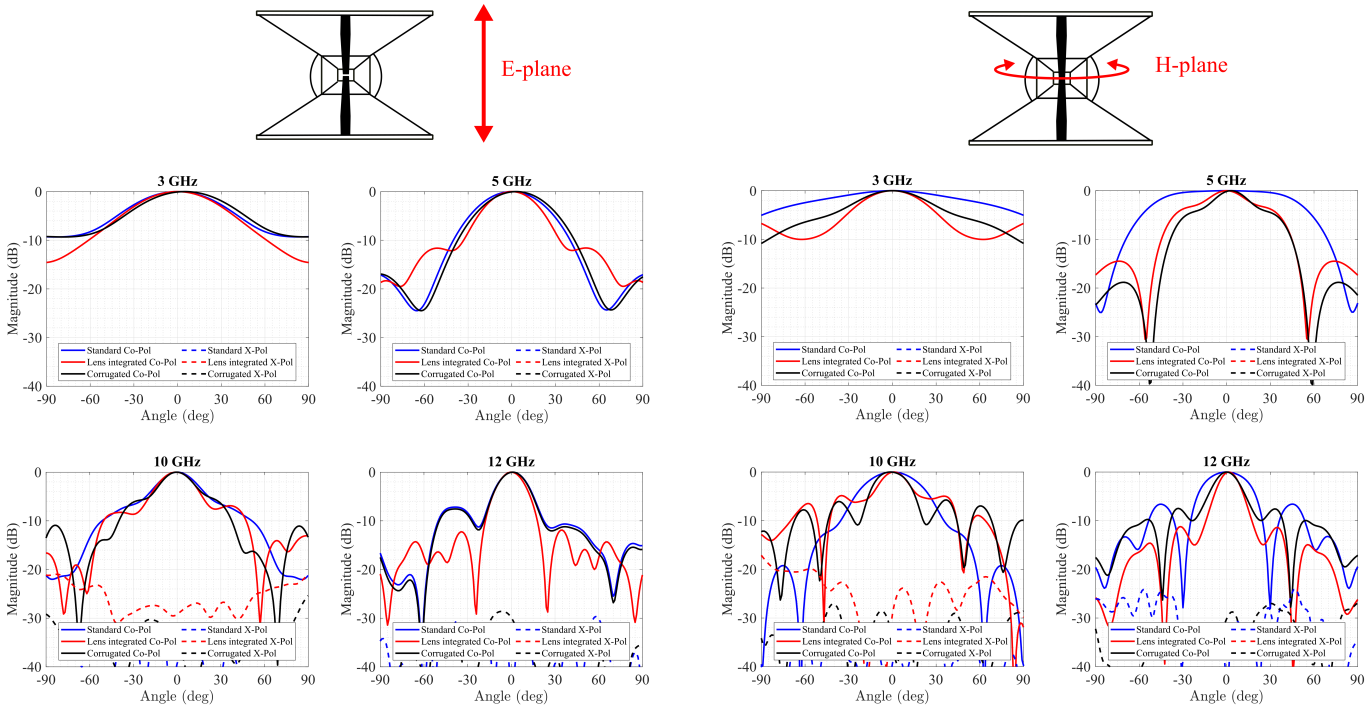

Fig. 5: Comparison of the simulated radiation patterns for the three cases (considering only antennas), in both planes and at different frequencies.

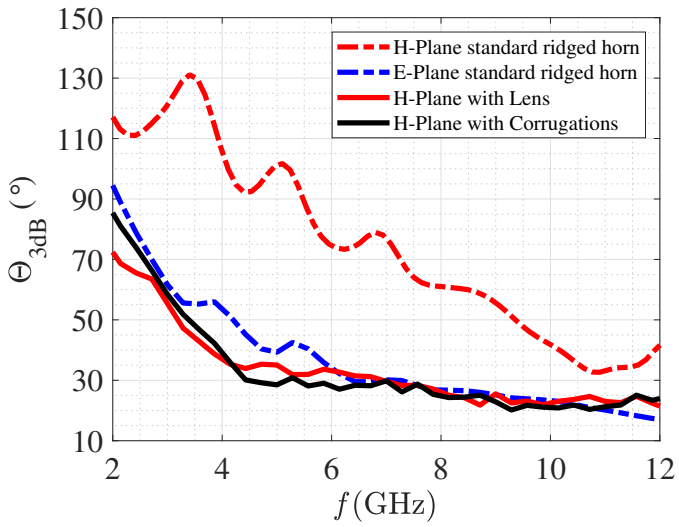

Fig. 6: Comparison of the simulated 3dB beamwidths for the three cases (for E-plane only one curve is shown since the lens or the corrugation does not significantly affect the E-plane beamwidth performance).

cavity structure that improves the matching performance. The ridged structure of the horn increases the electrical length of the waveguide aperture and thus lowers the dominant mode propagation inside the waveguide which significantly increases the bandwidth of the antenna. The corrugations behave as a capacitive reactive surface where the tangential component of the magnetic field is zero. Such a surface does not support surface waves, minimize diffractions, and prevents illumination from the edges, thus improving the side-lobe level and the beamwidth performance.

III. The Need for Narrow Beamwidth at Low Frequencies: Preliminary Results

The proposed measurement setup explained in the previous section, was used inside the anechoic chamber to characterize the SH2000 dual ridged horn antenna. For illustration, radiation patterns at the lower and the upper frequency bands are shown in both E and H planes and for both polarizations: vertical polarization (V-Polarized) and horizontal polarization (H-Polarized). These results are shown in Figs. 3 and 4. From these figures, it can be seen that when the antenna is V-Polarized (Fig. 3), the boresight cross-polarization for the drone case is less than -25 dB at low frequencies in both E and H planes. However, when the antenna is H-Polarized as shown in Fig. 4, the cross-polarization for the drone case gets worse at low frequencies especially in the H-pane where it is around -16 dB. This is due to the fact that at low frequencies, the beamwidth is wider and the fields strongly interact with the drone structure and creates some ripples in the co-polar patterns as well as increase the cross-polarization contamination. On the other hand, at higher frequencies, for both polarizations, the cross-polarization levels are not significantly affected because the beamwidth at higher frequencies is narrower in both planes, and thus the scattering from the UAV platform is minimum. This analysis necessitates the need for symmetric radiation patterns and reduction in the beamwidth performance.

Fig. 5 shows the comparison of the simulated radiation patterns of the antenna for the three cases at different frequencies.

The results for only one polarization are shown since the drone is not included in this case and both polarization will have exactly the same performance in the simulations. From the figure, it can be seen that in E-plane, no obvious difference can be observed in the 3 dB beamwidths at various frequencies. However, in the H-plane, the beamwidth is significantly reduced in both lens and corrugated cases compared to the standard ridged horn case.

Fig. 6 shows and compares the simulated 3dB beamwidth curves of the H-plane for the three cases: standard ridged horn, ridged horn with an integrated lens, ridged horn with corrugations in the plates. Since the E-plane performance is not significantly affected by any of these techniques, a single E-plane curve is shown to avoid redundancy. From the figure, it can be seen that both of these techniques reduce the H-plane beamwidth in the entire band of operation. For instance, the reduction is around 70% for the low-frequency band at 3 GHz. Overall, after reduction in the H-plane beamwidth, the patterns seem to be nearly symmetric in the entire band of operation. This is also verified from the fields distributions on the aperture as shown in Fig. 1.

IV. Conclusion

Ridged horn antennas are useful for UAV-based measurements since they offer wide bandwidth and a compact size. A single wideband ridged horn probe can be used for phased array radars in the S, C, and X bands, instead of using multiple probes for characterization and measurements. This is cost-effective and time-saving. However, on the dark side, these ridged horn antennas suffer from wider beamwidth performance, especially at low frequencies. We have verified from the measured results that at low frequencies, when the beamwidth is wider, the fields strongly interact with the drone platform, thus induces ripples in the co-polar patterns and also increasing the cross-polarization levels, especially in the H-plane. To overcome this, we have proposed and analyzed two techniques to reduce the H-plane beamwidth by almost 70% at 3 GHz and to achieve beam constancy as well as symmetry in the patterns. The first technique is based on integrating a multi-layer dielectric lens structure while the second technique involves using corrugations in the plates of the ridged horn antenna. Both of these techniques exhibit similar performance in the entire band of operation from 2-12 GHz. Due to their similar performance, the corrugation technique can be advocated since fabricating a multi-layer dielectric lens would be challenging compared to fabricating a corrugated ridged horn. Moreover, a multi-layer dielectric lens will have material losses, increased size, and weight that can significantly affect the flight performance of the drone.

Acknowledgment

The authors would like to thank the Advanced Radar Research Center (ARRC) of The University of Oklahoma for providing the facilities needed to perform this research. They also thank the Phased Array Antenna Research and Development group (PAARD) members for the discussions and positive feedback.

References

[1] E. E. A. S. Committee, "IEEE standard test procedures for antennas," *ANSI/IEEE Std*, vol. 149, pp. 1–144, 1979.

[2] J. Hollis, T. Lyon, and L. Clayton, "Microwave antenna measurements, scientific-atlanta," *Inc., Atlanta, GA*, 1985.

[3] F. Paonessa, G. Virone, P. Bolli, G. Pupillo, J. Monari, F. Perini, A. Mattana, G. Naldi, M. Poloni, M. Schiaffino *et al.*, "The UAV-based test source as an end-to-end verification tool for aperture arrays," in *2016 International Conference on Electromagnetics in Advanced Applications (ICEAA)*. IEEE, 2016, pp. 886–889.

[4] F. Paonessa, G. Virone, I. Aicardi, A. Lingua, M. Piras, P. Maschio, P. Bolli, G. Addamo, O. Peverini, R. Orta *et al.*, "Recent results in antenna pattern measurement with UAVs," in *2015 International Conference on Electromagnetics in Advanced Applications (ICEAA)*. IEEE, 2015, pp. 720–721.

[5] G. Virone, F. Paonessa, A. Tibaldi, Z. Farooqui, G. Addamo, O. A. Peverini, R. Tascone, P. Bolli, A. Mattana, J. Monari *et al.*, "UAV-based radiation pattern verification for a small low-frequency array," in *2014 IEEE Antennas and Propagation Society International Symposium (APSURSI)*. IEEE, 2014, pp. 995–996.

[6] F. Üstüner, E. Aydemir, E. Güleç, M. İlarslan, M. Çelebi, and E. Demirel, "Antenna radiation pattern measurement using an unmanned aerial vehicle (UAV)," in *2014 XXXIth URSI General Assembly and Scientific Symposium (URSI GASS)*. IEEE, 2014, pp. 1–4.

[7] A. M. Picar, C. Marqué, M. Anciaux, H. Lamy, and S. Ranvier, "Antenna pattern calibration of radio telescopes using an UAV-based device," in *2015 International Conference on Electromagnetics in Advanced Applications (ICEAA)*. IEEE, 2015, pp. 981–984.

[8] S. Duthoit, J. L. Salazar, W. Doyle, A. Segales, B. Wolf, C. Fulton, and P. Chilson, "A new approach for in-situ antenna characterization, radome inspection and radar calibration, using an unmanned aircraft system (UAS)," in *2017 IEEE Radar Conference (RadarConf)*. IEEE, 2017, pp. 0669–0674.

[9] J. L. Salazar, A. Umeyama, S. Duthoit, and C. Fulton, "UAS-based antenna pattern measurements and radar characterization," in *2018 IEEE Conference on Antenna Measurements & Applications (CAMA)*. IEEE, 2018, pp. 1–4.

[10] A. Y. Umeyama, J. L. Salazar-Cerreno, and C. J. Fulton, "UAV-based far-field antenna pattern measurement method for polarimetric weather radars: Simulation and error analysis," *IEEE Access*, vol. 8, pp. 191 124–191 137, 2020.

[11] A. Y. Umeyama, J. L. Salazar-Cerreno, and C. Fulton, "UAV-based antenna measurements for polarimetric weather radars: Probe analysis," *IEEE Access*, vol. 8, pp. 191 862–191 874, 2020.

[12] M. García-Fernández, Y. Á. López, A. Arboleya, B. González-Valdés, Y. Rodríguez-Vaqueiro, M. E. D. C. Gómez, and F. L.-H. Andrés, "Antenna diagnostics and characterization using unmanned aerial vehicles," *IEEE Access*, vol. 5, pp. 23 563–23 575, 2017.

[13] M. Garcia-Fernandez, Y. Alvarez-Lopez, and F. Las-Heras, "UAV-based antenna measurement and diagnostics for circularly polarized antenna arrays," in *2018 IEEE International Symposium on Antennas and Propagation & USNC/URSI National Radio Science Meeting*. IEEE, 2018, pp. 525–526.

[14] M. García Fernández, Y. Álvarez López, and F. Las-Heras, "Dual-probe near-field phaseless antenna measurement system on board a UAV," *Sensors*, vol. 19, no. 21, p. 4663, 2019.

[15] M. G. Fernandez, Y. A. Lopez, and F. L.-H. Andres, "On the use of unmanned aerial vehicles for antenna and coverage diagnostics in mobile networks," *IEEE Communications Magazine*, vol. 56, no. 7, pp. 72–78, 2018.

[16] J. L. Salazar-Cerreno, S. S. Jehangir, N. Aboserwal, A. Segales, and Z. Qamar, "An uav-based polarimetric antenna measurements for radar and communication systems from 3 ghz to 32 ghz," in *2021 IEEE Conference on Antenna Measurements Applications (CAMA)*, 2021, pp. 55–60.

[17] S. S. Jehangir, Z. Qamar, N. Aboserwal, and J. L. Salazar-Cerreno, "Application of the mixing theory in the design of a high-performance dielectric substrate for microwave and mm-wave systems," *IEEE Access*, vol. 8, pp. 180 855–180 868, 2020.